Renitence vacuoles facilitate protection against phagolysosomal damage in activated macrophages

Amanda O. Wong[a,b], Matangi Marthi[c], Zachary I. Mendel[c], Brian Gregorka[c], Michele S. Swanson[c], and Joel A. Swanson[a,c,*]

[a]Immunology Graduate Program, [b]Medical Scientist Training Program, and [c]Department of Microbiology and Immunology, University of Michigan Medical School, Ann Arbor, MI 48109

ABSTRACT As professional phagocytes, macrophages are susceptible to endolysosomal membrane damage inflicted by the pathogens and noxious particles they ingest. Whether macrophages have mechanisms for limiting such damage is not well understood. Previously, we reported a phenomenon, termed "inducible renitence," in which lipopolysaccharide (LPS) activation of macrophages protected their endolysosomes against damage initiated by the phagocytosis of silica beads. To gain mechanistic insight into the process, we analyzed the kinetics of renitence and morphological features of LPS-activated versus resting macrophages following silica bead–mediated injury. We discovered novel vacuolar structures that form in LPS-activated but not resting macrophages following silica bead phagocytosis. Because of their correlation with renitence and damage-resistant nature, we termed these structures "renitence vacuoles" (RVs). RVs formed coincident with silica bead uptake in a process associated with membrane ruffling and macropinocytosis. However, unlike normal macropinosomes (MPs), which shrink within 20 min of formation, RVs persisted around bead-containing phagosomes. RVs fused with lysosomes, whereas associated phagosomes typically did not. These findings are consistent with a model in which RVs, as persistent MPs, prevent fusion between damaged phagosomes and intact lysosomes and thereby preserve endolysosomal integrity.

INTRODUCTION

In multicellular organisms, phagocytosis is principally performed by specialized cells such as macrophages, which serve homeostatic and immune roles through the clearance of apoptotic bodies, par-ticulate matter, and pathogenic microbes. As much of the material that macrophages ingest has the potential to perforate phagolyso-somes, mechanisms to mitigate such damage likely exist. Innate immune responses to pathogen-mediated phagolysosomal injury include the sequestration of escaped pathogens or damaged phagolysosomes by autophagy (Levine *et al.*, 2011) and the triggering of pro-inflammatory responses after the cytosolic sensing of pathogens or their products by inflammasomes (Schroder and Tschopp, 2010). However, whether cellular mechanisms exist for preventing phagolysosomal injury from occurring in the first place is not known.

Earlier work demonstrated that macrophages primed against infection can reinforce their lysosomal integrity. Using a ratiometric fluorescence microscopic assay for measuring lysosomal damage in macrophages, we discovered that macrophages exposed to lipopolysaccharide (LPS), interferon γ (IFN-γ), heat-killed *Listeria monocytogenes* (*L.m.*), or other host and microbial factors associated with macrophage activation were better protected from lysosomal damage initiated by phagocytosis of acid-washed (AW)

silica beads than were unstimulated, resting macrophages (Davis *et al.*, 2012). This protection against lysosomal damage conferred by macrophage activation we termed "renitence." As LPS activation of macrophages up-regulates a number of antimicrobial activities, including reactive oxygen species production, autophagy, inflammasome priming, and cytokine secretion, we propose that renitence represents another measure within LPS-activated macrophages that increases resistance to infection by pathogens capable of perforating phagolysosomes. How cells might reinforce their endolysosomal compartments in anticipation of potentially injurious threats is a fundamental but poorly understood cell biological question that has primarily been studied using pathogens as agents of damage.

Recent studies of host factors that affect the integrity of bacteria-containing phagosomes in macrophages implicate endocytic processes in the maintenance of vacuolar integrity. IFN-γ activation of macrophages preserves the integrity of phagosomes containing *Mycobacterium tuberculosis* (Mtb) through regulating the spaciousness of Mtb-containing phagosomes (Schnettger *et al.*, 2017). That is, Mtb, as well as other microbes, can enter macrophages either in tight-fitting phagosomes, in which the incoming bacterium is tightly enclosed by the phagosomal membrane, or spacious phagosomes, enlarged compartments in which the bacterium and phagosomal membrane are separated by aqueous space (Case *et al.*, 2016). IFN-γ treatment increases the frequency with which Mtb is internalized into spacious phagosomes, which are less permissive to disruption than the tight phagosomes formed in resting macrophages (Schnettger *et al.*, 2017). The generation of spacious phagosomes in IFN-γ–activated macrophages was associated with an influx of endocytic vesicles following Mtb infection. This work thus established a link between macrophage activation, increased endocytic activity, spacious phagosome formation, and protection against pathogen-induced membrane injury.

Other examples of increased endocytic activity and spacious phagosome formation affecting phagolysosomal integrity or bacterial survival have been described, but usually in terms of the benefit for the pathogen. Infection of macrophages with *Salmonella typhimurium* (*S. Tm*), another intracellular pathogen capable of perforating phagosomes, induces generalized membrane ruffling and macropinocytosis, an endocytic process for the nonselective uptake of extracellular fluid (Alpuche-Aranda *et al.*, 1994; Swanson and Watts, 1995). Depending on its opsonization status, *S.Tm* is internalized by macrophages either into spacious phagosomes, which are morphologically identical to and likely represent macropinosomes (MPs), or into tight-fitting phagosomes that become spacious upon fusion with MPs (Alpuche-Aranda *et al.*, 1994). As *S. Tm* mutants lacking a specific virulence factor fail to induce spacious phagosome formation and are also defective for survival, spacious phagosome formation was found to promote *Salmonella* survival within macrophages. Thus, whereas spacious phagosomes harboring Mtb are host-protective through promoting maintenance of phagosome integrity (Schnettger *et al.*, 2017), those containing *S. Tm* appear to be necessary for survival of the pathogen (Alpuche-Aranda *et al.*, 1994). Macropinocytosis also contributes to the virulence of *Legionella pneumophila* (Watarai *et al.*, 2001) and *Shigella flexneri* (Weiner *et al.*, 2016).

The studies cited here provide evidence for a link between endocytic vesicle formation and phagolysosomal injury. Whether the connection is protective or deleterious to the host likely depends on the interplay between host and microbial factors. Not known is whether the host response to phagolysosomal damage caused by pathogens represents a general mechanism that reinforces endolyso-

somes against multiple forms of membrane injury. To examine host responses to membrane damage in the absence of confounding effects of virulence factor expression by pathogens, we used silica beads as an agent for inducing phagolysosomal injury. Phagocytosis of silica beads by macrophages induces membrane damage leading to the cytoplasmic release of fluorescent probes preloaded into endolysosomes, detectable by ratiometric imaging as an increase in the signal intensity of a pH-sensitive probe (Davis *et al.*, 2012; Joshi *et al.*, 2015).

Using this experimental system, we investigated the cellular mechanisms by which LPS stimulation of macrophages confers protection against lysosomal damage. We first identified key differences in the kinetics of the response of LPS-activated versus resting macrophages to silica bead–mediated injury and the size range of molecules released after bead challenge. Morphological comparison of resting versus LPS-treated macrophages led us to discover a structural correlate of renitence: large, damage-resistant vacuoles positioned adjacent to bead-containing phagosomes. These structures, which we term "renitence vacuoles" (RVs), resembled spacious phagosomes. Here, we report the dynamics of RV formation and their contribution to lysosomal damage protection by renitence. Overall, this work characterizes the responses of resting and LPS-activated macrophages to lysosomal injury and provides evidence for a model in which endocytic processes aid in the protection against lysosomal damage in activated macrophages.

RESULTS

LPS stimulation alters the time course of phagocytosis-mediated lysosomal damage

Damage to lysosomes within live murine bone marrow–derived macrophages (BMM) was measured using a ratiometric fluorescence microscopy assay developed previously (Davis and Swanson, 2010). Briefly, BMM whose lysosomes were pulse–chase labeled with the pH-sensitive dye fluorescein dextran (Fdx), were fed 3-μm AW silica beads (AW beads) at various time points to induce phagolysosomal damage. Fluorescence micrographs captured through exciting Fdx at its pH-sensitive (ex. 490 nm) and pH-insensitive (ex. 440 nm) wavelengths were used to determine ratiometrically the pH of intracellular regions containing the dye. Pseudocolor pH maps were generated to depict the pH within any subregion of the cell. Representative pseudocolor pH maps and the component images used to generate them for resting and LPS-treated BMM after 60 min of AW-bead incubation are shown in Figure 1A. Warm colors represent dye localized within acidic (i.e., lysosomal) regions, and cool colors represent dye that has entered pH-neutral (i.e., cytoplasmic) regions. Using the pH map to infer Fdx localization, lysosomal damage was quantified as the percent of Fdx pixels residing in regions whose pH was greater than 5.5, a measure that represents the extent of Fdx released from acidic lysosomes into the pH-neutral cytosol.

To characterize the kinetics of lysosomal damage and LPS-mediated protection following silica bead–mediated injury, we performed a time course of bead-mediated damage in resting versus LPS-activated macrophages. Lysosomal damage was compared in resting and LPS-treated cells that had internalized a similar number of beads (specifically, three to seven beads per cell). Damage measurements were made within individual cells (typically more than 100 cells per condition across three or more independent experiments) and reported as the average percent of Fdx release per cell for each condition.
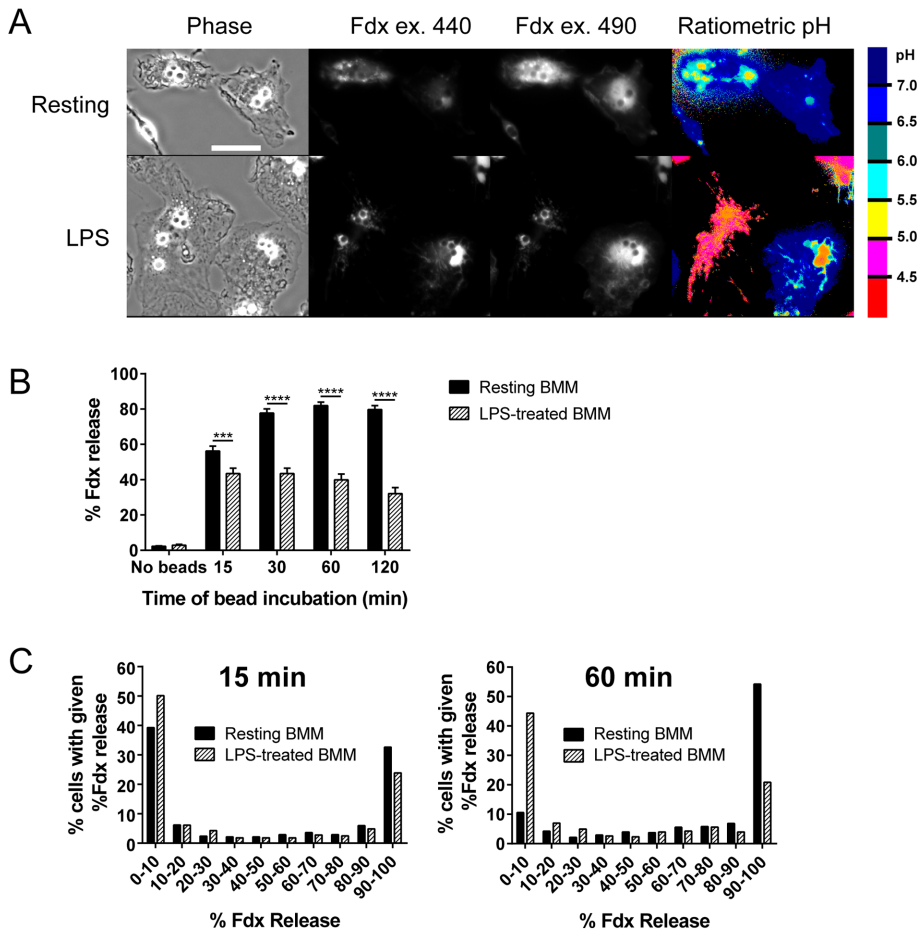
FIGURE 1: LPS stimulation limits the time window of phagocytosis-mediated damage to macrophage lysosomes. Lysosomes within resting and LPS-treated murine BMM were pulse–chase labeled with Fdx. (A) BMM were fed 3-µm AW silica beads (AW beads) for 60 min to induce phagolysosomal damage, and then epifluorescence images were collected to determine the extent of Fdx release from lysosomes into the cell cytoplasm. Representative phase-contrast and Fdx fluorescence images of resting (top) and LPS-treated (bottom) BMM are shown. Ratiometric, pseudocolor pH maps were generated by converting the ratio of ex. 490 nm/ex. 440 nm fluorescence intensities to pH values. Each Fdx pixel was then assigned a color corresponding to its pH value, with warm colors (e.g., red) representing dye within acidic regions (i.e., lysosomes) and cool colors (e.g., blue) representing dye in the pH-neutral cytosol. The extent of this release was quantified as the percent of Fdx pixels residing in regions whose pH was greater than 5.5. Resting BMM challenged with AW beads released large amounts of Fdx into the cytoplasm (left cell: 81% release; right cell: 100% release), whereas BMM pretreated with LPS exhibited much less release (left cell: 0.1% release; right cell: 56% release). Scale bar: 10 µm. (B) Time course of AW bead–mediated lysosomal damage in resting or LPS-treated mouse BMM. Release of Fdx from prelabeled lysosomes was measured on a per cell basis after BMM were incubated with AW beads for the indicated times. Bars show average percent Fdx release per cell ± SEM from four independent experiments, in which cells containing three to seven beads were analyzed ($n > 120$ cells). ***, $p \le 0.001$; ****, $p \le 0.0001$. (C) Individual cell data from A plotted in histogram form to show the percent of cells within each condition experiencing a given range of lysosomal damage (represented in 10% increments on the x-axis) after 15 (left) or 60 (right) min of exposure to AW beads.

Whereas resting macrophages experienced increasing levels of damage over time, proceeding to near-complete dye release, LPS-activated macrophages restricted damage to the first 15 min of bead challenge (Figure 1B). After incurring an initial damaging insult, LPS-activated macrophages either limited further progression of damage or quickly repaired the original breach. Thus, the basis of protection in LPS-activated macrophages lies in activities that preserve lysosomal integrity after the first 15 min of damage initiation.

## LPS stimulation protects against all-or-none damage by silica beads

As our damage measurements were made on a per cell basis, we could achieve a more granular analysis by plotting in histogram form the distribution of damage levels measured from the individual cells contributing to the average Fdx release data. The histograms depict the proportion of cells in each condition experiencing a given range of damage after exposure to beads for 15 or 60 min (Figure 1C). By this analysis, we discovered that damage caused by AW beads in both resting and LPS-treated BMM resulted mostly in either complete (90–100%) or negligible (0–10%) dye release. Only a small proportion of cells (<30%) experienced levels of dye release between these two extremes.

The progression of damage between 15 and 60 min of bead incubation seen at the population level in resting macrophages was accounted for by a reduction in the proportion of cells experiencing low levels of damage and an increase in the proportion of cells experiencing high levels of damage. This shift was resisted in LPS-treated macrophages. Two major conclusions were drawn from these analyses: 1) lysosomal damage caused by AW beads was largely all-or-none; and 2) LPS-stimulated macrophages experienced damage heterogeneously; one population showed near-complete damage within 15 min of receiving beads, whereas another resisted damage throughout the course of bead incubation. LPS-stimulated macrophages therefore restrict damage to a narrow time window by preventing a protected population of cells from undergoing damage.

Silica bead uptake initiates small membrane breaches

We next determined the size of the membrane breaches formed by ingested AW beads and the size dependence of LPS-induced renitence. To address these questions, we measured the upper size limit of Fdx molecules released from lysosomes after bead-mediated injury. Macrophage lysosomes were loaded with fluorescein dextran molecules of various molecular weights, ranging from 3 kDa (the size of dye used in our standard damage assays) to 70 kDa Fdx, and then subjected to 60 min of AW-bead incubation. To represent the unusually large variation in damage between experimental replicates for certain conditions, we plotted Fdx release values for individual experimental replicates along with the average percent Fdx release for a given condition (Figure 2).

While leakage of 3-kDa Fdx from lysosomes occurred readily, the release of the two largest dyes tested (40 and 70 kDa) was much more limited in both resting and LPS-treated BMM. Thus, AW-bead
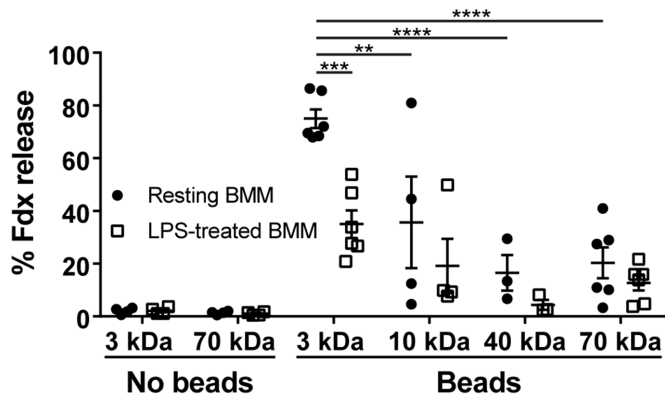
FIGURE 2: Silica bead uptake induces membrane injury that permits the release of small but not large molecules. Lysosomes within resting or LPS-treated BMM were pulse–chase labeled with Fdx molecules of different sizes: 3, 10, 40, or 70 kDa. The extent of Fdx release after 60 min of AW-bead incubation was measured for each group of cells in at least three independent experiments. Fdx release values from individual experiments are plotted along with the average percent Fdx release ± SEM across all replicates. In all bead-positive conditions, cells containing three to seven beads were analyzed ($n > 35$ cells within each individual experiment). **, $p \leq 0.01$; ***, $p \leq 0.001$; ****, $p \leq 0.0001$.

uptake induces the release of small but not large dyes from lysosomes irrespective of macrophage activation state. To define more precisely the size of the membrane breach, the release of a dye of an intermediate size (10-kDa Fdx) from prelabeled lysosomes was monitored. The extent of 10-kDa Fdx release varied significantly between experimental replicates, with resting macrophages exhibiting high levels of release in two experiments but low levels of release in two others. The upper size limit of molecule release therefore likely lies between 10 and 40 kDa. These data indicate that silica bead uptake initiates small but not large membrane breaches to lysosomes. As no statistically significant differences were noted in the extent of release of dyes ≥10 kDa in resting versus LPS-treated BMM, renitence likewise preferentially counteracts the formation of small but not large membrane breaches.

Damage-resistant vacuoles are formed in response to phagolysosomal injury in LPS-activated macrophages

To uncover mechanistic details of renitence, we compared morphological features of resting versus LPS-treated macrophages following AW-bead uptake. Using phase-contrast and ratiometric fluorescence images, we correlated states of damage or protection with cell morphology. By analyzing profiles of hundreds of cells, we noticed a distinct morphological feature common to LPS-treated macrophages, but rarely seen in resting macrophages. After a 60-min incubation with AW beads, LPS-treated macrophages often contained large, vacuolar structures adjacent to bead-containing phagosomes (Figure 3A). These vacuoles were visible on phase-contrast images as circumscribed phase-dense regions adjacent to internalized beads. They often contained Fdx, suggesting their origin as, or fusion with, lysosomes. Most strikingly, in pseudocolor pH images, these vacuoles were the most acidic Fdx-labeled regions within cells (Figure 3A). Even in cells in which most of the lysosomal network was damaged, as judged by the localization of Fdx in pH-neutral regions, the vacuoles persisted as intact, acidic structures.

The acidic content of vacuoles, despite their proximity to membrane-damaging beads, suggested a possible protective function. To interrogate the role of vacuoles in mediating protection, we first

enumerated vacuole frequency in resting and LPS-treated BMM after a 60-min incubation with AW beads. Vacuoles were scored as phase-dense structures that contained Fdx and appeared adjacent to an internalized bead. Analyzing more than 2500 cells per condition, we found that AW-bead incubation induced vacuole formation in ~25% of LPS-treated BMM, but in less than 10% of resting BMM (Figure 3B). To determine whether vacuole formation required membrane damage, we assessed vacuole frequency in cells fed damaging versus nondamaging beads. Nondamaging beads were generated by conjugating AW silica beads to bovine serum albumin (BSA), which attenuates damage, presumably by neutralizing the damage-inducing surface properties of the silica beads. Indeed, administration of BSA-coated beads induced very low levels of injury (Figure 3C). Correspondingly, few vacuoles were observed (Figure 3D), suggesting that vacuole formation occurred specifically in response to membrane damage.

Damaging bead uptake induces RV and MP formation in LPS-activated but not resting macrophages

To capture the dynamics of vacuole formation, we performed time-lapse imaging of resting versus LPS-treated BMM immediately following their incubation with AW beads. Before imaging, lysosomes within BMM were pulse-chase labeled with the fluid-phase probe Lucifer yellow (LY). Upon bead addition, phase-contrast and LY fluorescence images were captured every 20 s for 1 h. The resulting movies revealed that phagocytosis of AW beads in LPS-treated but not resting BMM was accompanied by the formation of phase-bright vacuoles associated with phagosomes. In a representative movie of an LPS-activated macrophage, multiple vacuoles surrounding a bead-containing phagosome appeared within 7 min after bead incubation (Figure 4 and Supplemental Videos S1 and S2). Some vacuoles received LY from lysosomes, indicating their ability to fuse with lysosomes. Notably, the vacuoles did not shrink but instead persisted around the bead throughout its course of trafficking in the cell. The early appearance of vacuoles following bead uptake and their prolonged persistence were observed in multiple cells.

Coincident with bead phagocytosis and vacuole formation, LPS-treated macrophages underwent vigorous membrane ruffling leading to the formation of numerous phase-bright structures in the cell. These structures resembled macropinosomes (MPs), vesicles formed through a form of fluid-phase endocytosis called macropinocytosis (Swanson and Watts, 1995). The large size of vacuoles, their coincident appearance with MPs, and their persistence near a bead even 60 min after administration suggested that they form as MPs that enlarge and persist near phagolysosomes in the context of membrane injury. No vacuoles and few MPs were observed within resting macrophages, which did however undergo continuous membrane ruffling upon bead incubation (Figure 4A). As the vacuoles observed by time-lapse microscopy share many characteristics with those quantified in fixed time-point analyses in Figure 3, they both likely are of the same origin. We refer to these MP-like, periphagosomal organelles as "renitence vacuoles" (RVs).

RVs resembled spacious phagosomes (SPs) previously observed within macrophages infected with *S. Tm* (Alpuche-Aranda *et al.*, 1994). Although SP formation was thought to be induced by the bacteria to promote their survival within the host environment, our observation of a compartment of strikingly similar morphology in the setting of non–pathogen related membrane injury suggests that the structures form instead as a protective response in activated macrophages. In fact, evidence from time-lapse imaging of LPS-activated BMM fed nondamaging phagocytic targets suggests macropinocytosis and vacuole formation accompany phagocytosis
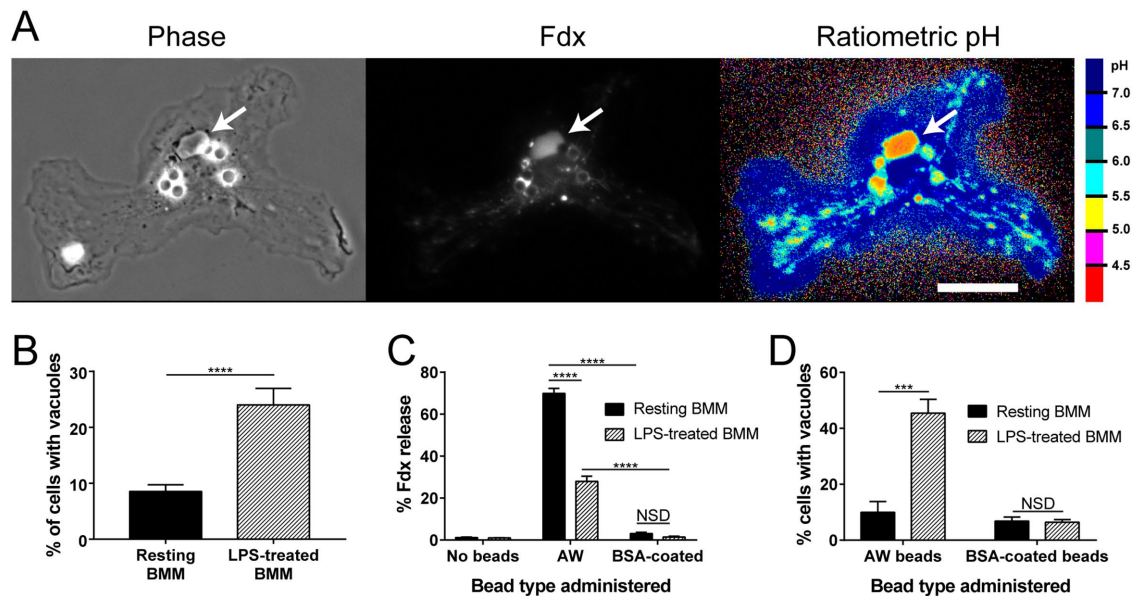
FIGURE 3: LPS-activated macrophages form damage-resistant vacuoles in response to phagolysosomal injury. (A) Phase-contrast, Fdx fluorescence (ex. 440 nm–em. 535 nm), and pseudocolor pH images of a representative LPS-treated macrophage harboring a damage-resistant vacuole, indicated with arrow. Scale bar: 10 μm. (B) Vacuole frequency in resting or LPS-treated BMM after 60 min of AW-bead incubation. Vacuoles were defined by the following criteria: 1) appearance on phase-contrast image as a circumscribed phase-dense region adjacent to an internalized bead, and 2) presence of Fdx within the structure. Each bar displays the average ± SEM of the percent of cells within each condition harboring one or more vacuoles. All cells containing at least one bead were analyzed. ($n = 27$ experiments, with more than 2500 cells analyzed.) ****, $p \leq 0.0001$. (C) Average percent Fdx release ± SEM from prelabeled lysosomes in resting or LPS-treated BMM after a 60-min incubation with damaging (AW) or nondamaging (BSA-coated) beads. Bars represent data from three experiments, in which cells containing three to seven beads per cell were analyzed ($n > 170$ cells). ****, $p \leq 0.0001$. (D) Vacuole frequency in resting or LPS-treated BMM after a 60-min incubation with damaging (AW) or nondamaging (BSA-coated beads). Analysis was performed on the set of images used to determine Fdx release values in C. Bars represent the mean percent ± SEM of cells containing one or more vacuoles. ***, $p \leq 0.001$.

generally. BMM fed either BSA-coated beads (Supplemental Figure S1A and Supplemental Videos S4 and S5), or immunoglobulin G–opsonized sheep red blood cells (sRBCs) (Supplemental Figure S1B and Supplemental Video S6), shown previously to be nondamaging to resting or LPS-treated BMM (Davis and Swanson, 2010), also induced the formation of vacuoles adjacent to the internalized bead or sRBC. In contrast, vacuoles were not observed in resting BMM fed nondamaging BSA-coated beads (Supplemental Figure S1C and Supplemental Video S7).

How might these results be reconciled with those in Figure 3D, in which few vacuoles were detected after a 60-min incubation with BSA-coated beads? The presence of vacuoles in dynamic analyses but their absence in static analyses suggested that vacuoles associated with nondamaging-bead phagocytosis typically form and shrink before the 60-min time point used for fixed time-point analysis. Consistent with this model, the vacuoles in videos capturing the phagocytosis of BSA-coated beads differed in two ways from RVs formed upon AW-bead uptake. First, while characteristic RVs formed coincident with AW-bead phagocytosis, the vacuoles accompanying BSA-coated bead phagocytosis formed more slowly, with a delay of several minutes between bead internalization and vacuole formation. Second, once formed, the vacuoles generally shrank quickly, like typical MPs (Supplemental Video S5). In only one of three independent experiments did we capture a large, bead-adjoining, persistent vacuole in an LPS-treated BMM fed BSA-coated beads (Supplemental Figure S1A and Supplemental

Video S4). These studies suggested that 1) MP and vacuole formation is induced by phagocytosis of damaging and nondamaging particles in LPS-activated macrophages, and 2) phagocytosis of damaging particles induces additional activities that cause RVs to persist.

Macropinocytosis is necessary for renitence

On the basis of our morphological findings, we hypothesized that RVs, as persistent MPs, contribute to renitence in LPS-activated macrophages. To interrogate the role of macropinocytosis in renitence, we first assessed the extent to which LPS activation of macrophages induces macropinocytosis. Using a microscopic assay for counting MPs, we observed that overnight LPS stimulation of BMM induced MP formation to a similar degree as that induced by acute stimulation with macrophage colony-stimulating factor (M-CSF) (Figure 5A), long known to induce macropinocytosis in macrophages (Racoosin and Swanson, 1989). Confirming that the endocytic vesicles counted were indeed MPs, treatment of LPS-activated BMM with the macropinocytosis inhibitor 5-(N-ethyl-N-isopropyl) amiloride (EIPA) reduced their formation.

The extent of macropinocytosis increased with the duration of LPS incubation, peaking after 6–18 h of LPS stimulation (Figure 5B). The time course of LPS-induced macropinocytosis strikingly paralleled the time course of LPS-induced renitence, in which protection was first seen in BMM after 6 h of LPS stimulation and peaked in BMM stimulated with LPS overnight (Davis et al., 2012). Thus, macropinocytosis
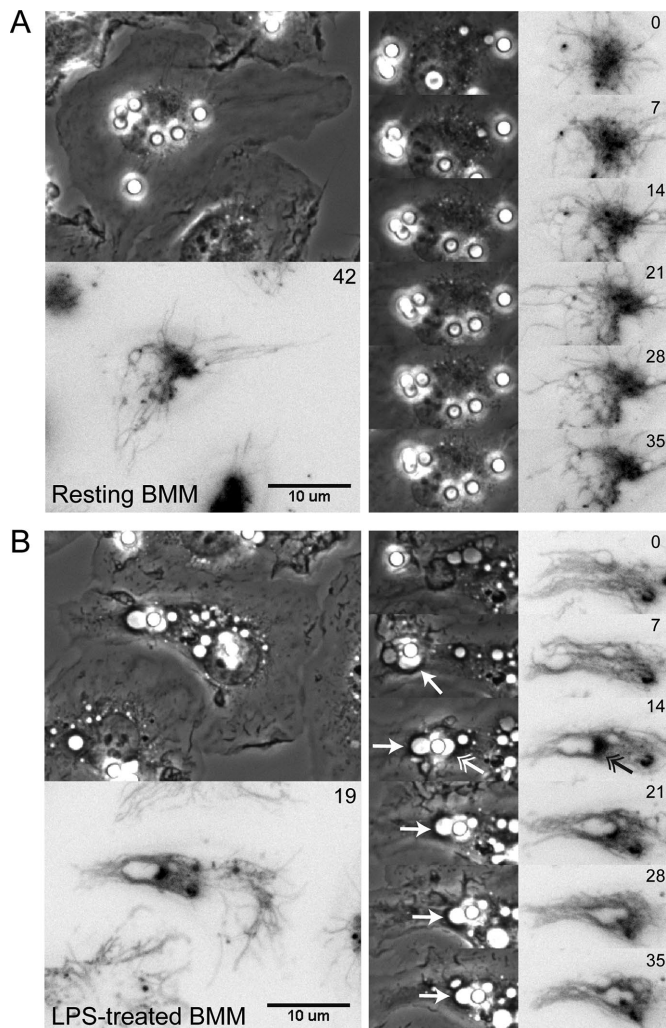
FIGURE 4: Damaging bead uptake induces RV and MP formation in LPS-treated but not resting macrophages. Resting (A) or LPS-treated (B) BMM whose lysosomes were labeled with LY were fed AW beads and imaged by time-lapse microscopy. Phase-contrast and LY fluorescence images were captured every 20 s for 1 h. Panels show selected frames of phase-contrast and inverted contrast LY fluorescence images from corresponding time points in the time series. Elapsed time in minutes after the addition of AW beads ($t = 0$ min) is shown in the top right of each subpanel. Single arrows in B mark regions in which numerous MPs and vacuoles surround an incoming phagosome, a characteristic event accompanying phagocytosis in LPS-treated BMM. Double arrow (B, 14 min) indicates a vacuole that has merged with and received LY from lysosomes. Scale bar: 10 μm.

is up-regulated following LPS stimulation, with a time course similar to that of renitence.

To investigate whether macropinocytosis and renitence are directly related, we next assessed the effect of macropinocytosis induction and inhibition on renitence. Induction of macropinocytosis through inclusion of M-CSF in the media at the time of AW-bead incubation led to a modest reduction in damage (Figure 5C). In contrast, inhibition of macropinocytosis by EIPA exacerbated damage in LPS-activated macrophages and significantly abrogated renitence (Figure 5D). These results suggested that macropinocytosis contributes to renitence in LPS-activated macrophages.

RVs originate as MPs and fuse with lysosomes

To investigate how MPs contribute to renitence, we visualized the dynamic interactions of MPs, RVs, bead-containing phagosomes, and lysosomes following silica bead uptake. Time-lapse video microscopy was performed in LPS-treated BMM whose lysosomal and endocytic compartments were labeled with different fluorescent probes. Texas Red dextran (TRDx; 70 kDa) labeling of lysosomes was followed by coadministration of AW beads and Fdx (70 kDa), which allowed for the labeling of MPs formed during bead phagocytosis. After a 5-min incubation with beads and Fdx, cells were washed to remove the extracellular probe and mounted for imaging by phase-contrast, Fdx, and TRDx fluorescence microscopy. Phase-contrast and fluorescence (TRDx, Fdx) images were taken every 20 s over 20 min to capture events occurring between 5 and 25 min post–AW bead incubation.

At the start of imaging, RVs had already formed and contained Fdx (Figure 6A and Supplemental Video S3), confirming their origin as MPs. RVs persisted next to bead-containing phagosomes through all time points imaged, long after normal MPs would have already shrunk (Racoosin and Swanson, 1993). These observations support the conclusion that RVs represent persistent MPs.

MP-derived RVs eventually fused with lysosomes, as evidenced by the acquisition of TRDx by RVs at later time points (Figure 6A and Supplemental Video S3). Fusion events for two separate RVs within a representative cell were noted 13 and 21 min after bead incubation (Figure 6A). RV acquisition of TRDx occurred within a similar time frame in multiple cells analyzed.

For following the fate of RVs after their fusion with lysosomes, time-lapse microscopy was performed on LPS-treated BMM as described above, but with imaging beginning 30 min after cells were exposed to AW beads. Using the same imaging intervals as in Figure 6A, events occurring between 30 and 50 min post–AW bead incubation were captured. RVs were shown to persist as Fdx-positive, TRDx-positive structures through these later time points (unpublished data). Together, these studies indicate that RVs originate as MPs, fuse with lysosomes, and persist as enlarged structures near AW bead–containing phagosomes.

RVs transition from Rab5-positive to LAMP-1–positive structures within 30 min

To further characterize the identity of RVs and the intracellular organelles with which they interact, we assessed the timing of recruitment to RVs of molecular markers of major organelles of the endolysosomal pathway. As fixation and permeabilization methods for immunofluorescence staining failed to preserve RV structures in fixed cells, we performed these studies in live BMM transfected with fluorescent chimeras of Rab5a, a marker of early endosomes, and LAMP-1, a marker of late endosomes and lysosomes. LPS-treated BMM expressing yellow fluorescent protein (YFP)-Rab5a, cyan fluorescent protein (CFP)-LAMP-1, and mCherry were incubated with AW beads for 5 or 20 min and then mounted for imaging by phase-contrast and ratiometric fluorescence microscopy. Still images of cells expressing all three probes were acquired over a 5-min imaging interval for coverslips exposed to beads for 5 min and over a 10-min imaging interval for coverslips exposed to beads for 20 min. Recruitment of Rab5a and/or LAMP-1 to RVs at either time point was determined using ratiometric images for each probe (i.e., YFP-Rab5a/mCherry and CFP-LAMP-1/mCherry). Representative component and ratiometric images used for analysis are shown in Figure 7.

In cells imaged between 5 and 10 min after AW-bead incubation, a mixed population of RVs was observed, with a comparable proportion of RVs having acquired Rab5 only, LAMP-1 only, or both
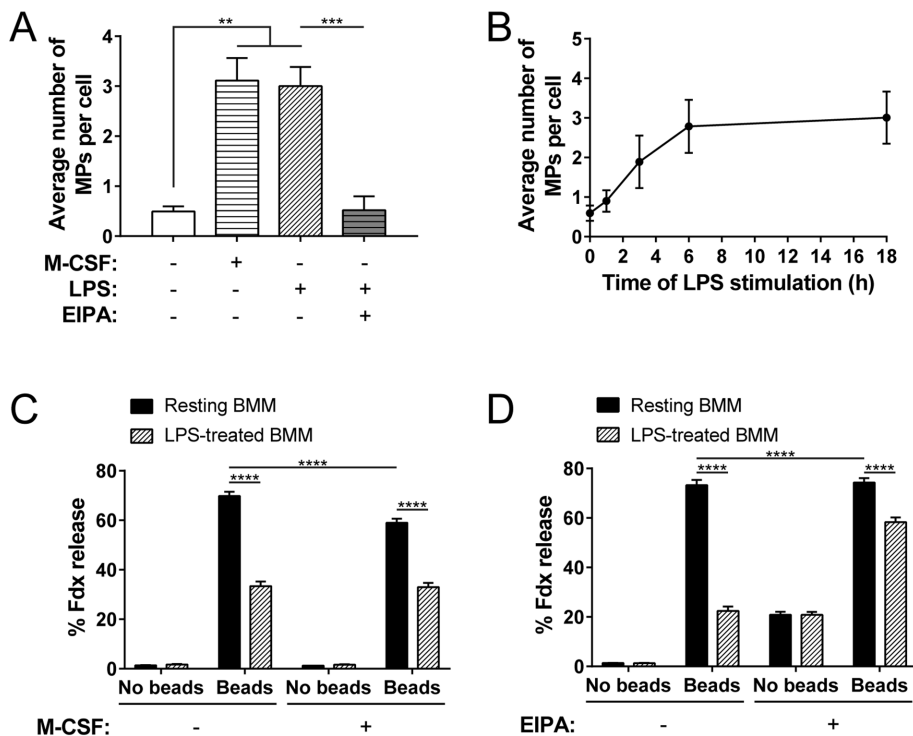
FIGURE 5: Macropinocytosis contributes to renitence. (A) Average MP number per cell ± SEM was measured in resting and LPS-treated BMM in the presence or absence of macropinocytosis stimulation by M-CSF or inhibition by EIPA. BMM were pulsed with 70-kDa Fdx for 10 min, then washed, fixed, and imaged by fluorescence microscopy. MPs were scored as phase-bright structures within cells that colocalized with 70-kDa Fdx. In control conditions, BMM were either stimulated for 10 min with M-CSF (200 ng/ml) during the Fdx pulse to induce macropinocytosis or pretreated for 30 min with EIPA (25 μM) before the start of the Fdx pulse to inhibit macropinocytosis. Data from four or more independent experiments are shown. **, $p \leq 0.01$; ***, $p \leq 0.001$. (B) Time course of LPS-induced macropinocytosis in macrophages. The average number of MPs per cell ± SEM was measured after exposure of cells to 70-kDa Fdx for 10 min in BMM treated with LPS for 1, 3, 6, or 18 h or left unstimulated (0 h). Data from at least three independent experiments are shown. (C) Average percent Fdx release ± SEM in resting or LPS-treated BMM fed AW beads for 60 min in the presence or absence of M-CSF to stimulate macropinocytosis. Bars represent data from three or more independent experiments ($n > 350$ cells). ****, $p \leq 0.0001$. (D) Average percent Fdx release ± SEM in resting or LPS-treated BMM pretreated or not for 30 min with EIPA, an inhibitor of macropinocytosis, before undergoing 60-min incubation with AW beads. Bars represent data from three or more independent experiments ($n > 200$ cells). ****, $p \leq 0.0001$.

probes (Figure 7C). After 20–30 min of AW-bead incubation, RVs were nearly uniformly LAMP-1–positive, Rab5-negative structures. These results suggest that RVs acquire Rab5 soon after their formation and transition into LAMP-1–positive, Rab5-negative compartments within 30 min. The observation of LAMP-1–positive RVs within 5 to 10 min after AW-bead incubation suggests rapid acquisition of LAMP-1 within a subset of RVs, consistent with the kinetics of MP maturation and fusion with tubular lysosomes reported previously (Racoosin and Swanson, 1993).

Fusion of RV-associated phagosomes with lysosomes is impaired

While RVs fused with lysosomes, bead-containing phagosomes localized adjacent to RVs frequently did not. In experiments for Figure 6A, we noticed that, while most phagosomes were surrounded by a ring of TRDx fluorescence, indicative of fusion with TRDx-positive lysosomes, phagosomes localized adjacent to RVs rarely received lysosomal labeling. Phagosomes of both types could appear within the same cell, as seen in the representative

image shown in Figure 6B. This image of an LPS-treated BMM containing TRDx-labeled lysosomes was acquired 34 min after incubation with AW beads and 70-kDa Fdx. In the cell, two bead-containing phagosomes, seen at the top of the image, were associated with RVs. While the RVs themselves clearly received TRDx from lysosomes ("TRDx" and "Merge"), the bead-containing phagosomes, denoted by asterisks, did not. In contrast, phagosomes in another region of the same cell did not associate with RVs but did fuse with lysosomes, as a ring of TRDx fluorescence appears around most beads in the region.

To analyze the association between phagosome position and the frequency of phagosome–lysosome fusion, we quantified the percent of RV-associated as opposed to non–RV associated phagosomes exhibiting fusion with TRDx-labeled lysosomes in LPS-treated BMM. After a 60-min incubation with AW beads, 80% of non–RV associated phagosomes, but only 32% of RV-associated phagosomes, had reached TRDx-labeled lysosomes (Figure 6C). Thus, while most non–RV associated phagosomes readily mature, phagosomes associated with RVs are significantly impaired in their fusion with lysosomes.

DISCUSSION
This work reports the discovery of RVs, damage-resistant structures formed in LPS-activated macrophages that protect against phagocytosis-mediated lysosomal injury. The rapid formation of RVs in the setting of membrane damage, their maintenance of low pH despite their proximity to a damaging particle, and their correlation with renitence provide evidence of a protective function. The dynamic interactions observed among RVs, MPs, phagosomes, and lysosomes suggested a model for how RVs form and confer protection against lysosomal damage (Figure 8): In LPS-activated macrophages, macropinocytosis accompanies the phagocytosis of both damaging and nondamaging particles. Upon phagocytosis of a damaging particle, multiple MPs form around the phagosome, and in some cases enlarge and persist. These persistent, periphagosomal MPs (i.e., RVs) fuse with lysosomes, whereas phagosomes associated with RVs typically do not. Thus, RVs prevent the fusion of their associated phagosomes with lysosomes. This activity, we propose, likely relates to the mechanism by which RVs protect against lysosomal damage. By preventing the fusion of damaged phagosomes with intact lysosomes, RVs would contain damage to early endocytic compartments and prevent the propagation of damage throughout the entire endolysosomal network. This strategy would represent an important protective mechanism not only for preserving the integrity of lysosomes, but also for restricting the release of lysosomal contents into the cytoplasm, a highly immunogenic event (Boya and Kroemer, 2008; Hornung et al., 2008).
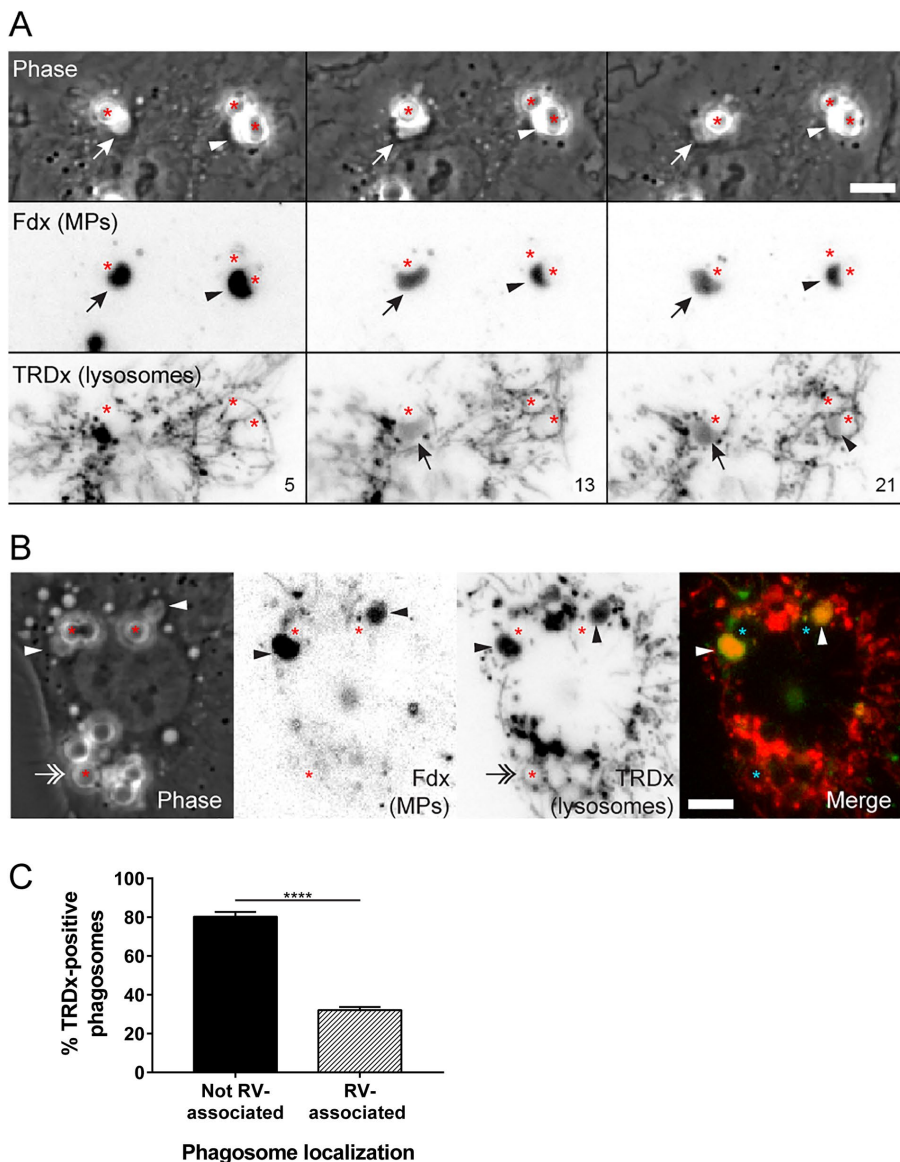
FIGURE 6: RVs are persistent MPs that fuse with lysosomes. (A, B) LPS-treated BMM whose lysosomes were prelabeled with 70-kDa TRDx were fed AW beads in media containing 0.5 mg/ml 70-kDa Fdx. After a 5-min incubation with beads and Fdx, samples were washed and mounted for time-lapse video microscopy. Phase-contrast and fluorescence images of endocytic (Fdx) and lysosomal (TRDx) compartments were taken every 20 s for 20 min. (A) Selected frames of phase-contrast and inverted-contrast Fdx and TRDx images capturing RVs before and after their mixing with lysosomes. Elapsed time in minutes after the addition of beads is indicated in the bottom right of each subpanel. Each arrow or arrowhead indicates a specific RV tracked between multiple frames. Asterisks denote the position of internalized beads. (B) Still frame of phase-contrast, Fdx, TRDx, and merged fluorescence images of an LPS-treated BMM captured 29 min after the initial 5-min incubation with AW beads and 70-kDa Fdx. Asterisks are positioned over bead-containing phagosomes. Arrowheads mark two representative RVs. Double arrow indicates region of internalized beads that are not associated with RVs. Scale bars: 10 μm. (C) Proportion of AW bead–containing phagosomes exhibiting fusion with lysosomes depending on the position of phagosomes relative to RVs (RVs). LPS-treated BMM containing 70-kDa TRDx-labeled lysosomes were fed AW beads for 60 min, washed to remove noninternalized beads, and then mounted for imaging. Within a 10-min imaging interval, at least 20 still frames of cells were captured by phase-contrast and fluorescence microscopy. Phagosomes were identified on phase-contrast micrographs and scored as either RV-associated or not. TRDx images were used to determine whether a given phagosome had fused with lysosomes, with fusion judged as TRDx localization around the internalized bead. The average percent ± SEM of phagosomes receiving TRDx labeling was quantified from micrographs acquired in three independent experiments, with triplicate coverslips serving as technical replicates in two of the three experiments ($n > 200$ phagosomes per coverslip). ****, $p \leq 0.0001$.

How might RVs interfere with the maturation of damaged phagosomes? RVs may act as decoy vesicles that fuse with lysosomes in lieu of damaged phagosomes. However, as RVs reside adjacent to, but do not completely surround, their neighboring phagosomes, it is unclear how lysosomes would be directed to preferentially fuse with RVs but not the exposed portion of the phagosome. An alternative hypothesis is that membrane damage, which induces RV formation, also induces cellular activities that render the phagosomal membrane incapable of exchanging membrane with downstream organelles of the conventional endocytic pathway. This could occur through the inactivation of trafficking proteins on the phagosomal membrane or through the exchange of these proteins from the phagosomal membrane to the RV membrane. In this model, an RV would not serve as a decoy vesicle, but as a signal that induces the cell to remove the phagosome from the normal route of maturation. While this study focused on the properties of RVs themselves and their role in preventing lysosomal damage, much remains to be learned about the fate of phagosomes following membrane damage.

A notable feature of RVs is their persistence. The persistence of RVs likely relates to their functional role, as conventional MPs and vacuoles formed during uptake of nondamaging beads eventually shrink. Thus, understanding the factors that govern RV persistence may help to elucidate the mechanism of renitence. As MPs formed in macrophages stimulated with M-CSF shrink via fusion with lysosomes within 15 min after their formation (Racoosin and Swanson, 1993), RV persistence may be caused by defects in their trafficking to lysosomes. However, as RVs readily recruit LAMP-1 and acquire fluorescent probes preloaded into lysosomes, this possibility seems unlikely. Alternatively, RVs might persist due to an inhibition of MP shrinkage by other mechanisms or by an increase in fluid influx into the vacuole.

MPs themselves could be a source of extracellular fluid that maintains vacuole persistence. Additionally, as membrane-bound vesicles, MPs could contribute membrane necessary for the expansion of the compartment. This work introduces several concepts connecting LPS activation, macropinocytosis, and renitence that are consistent with such a model. Macropinocytosis is induced robustly in LPS-activated macrophages and occurs both constitutively and following phagocytic challenge. In the case of damaging bead uptake, multiple MPs accumulate around the incoming phagosome. These
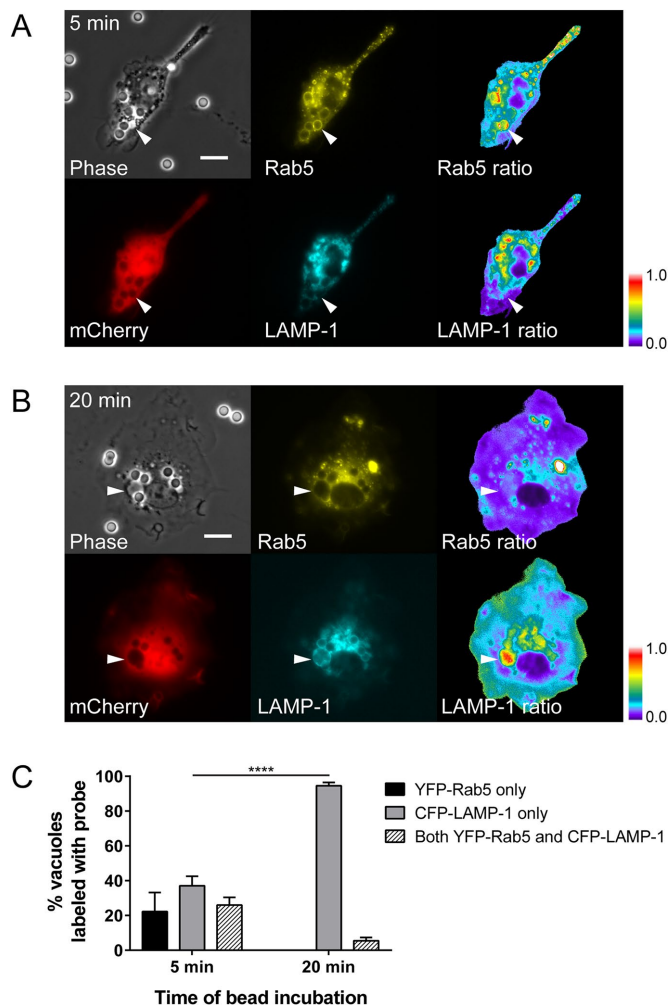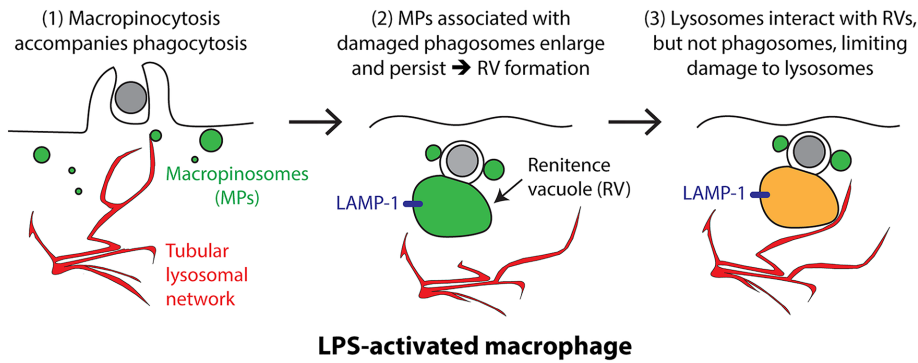
FIGURE 7: RVs transition from Rab5-positive to LAMP-1-positive structures within 30 min. BMM transfected with YFP-Rab5a, CFP-LAMP-1, and mCherry were stimulated overnight with LPS. After a 5-min (A) or 20-min (B) incubation with AW beads, cells were washed to remove noninternalized beads, then imaged by phase-contrast and ratiometric fluorescence microscopy. Multiple still frames of cells expressing all three probes were imaged within a 5- or 10-min time window following each period of bead incubation. Phase-contrast images were used to identify RVs. Ratiometric pseudocolor images (YFP-Rab5/mCherry and CFP-LAMP-1/mCherry) were used to assess probe recruitment to RVs. (A, B) Representative phase-contrast, fluorescence, and processed images of vacuole-containing LPS-treated BMM imaged between 5 and 10 min (A) or 20 and 30 min (B) after AW-bead incubation. Pseudocolor images show recruitment of Rab5 but not LAMP-1 to the RV (indicated with arrowhead) in A and, conversely, recruitment of LAMP-1 but not Rab5 to the RV (indicated with arrowhead) in B. Scale bar: 10 μm. (C) Proportion of RVs that had acquired YFP-Rab5, CFP-LAMP-1, or both probes within LPS-treated BMM imaged after incubation with AW beads. Bars show the average percent ± SEM of vacuoles labeled with probes from four independent experiments. Weighted averages were calculated, where data from replicates in which more vacuoles were observed were proportionally given more weight. A total of 27 vacuoles were analyzed for cells imaged within the 5- to 10-min time interval, and a total of 55 vacuoles were analyzed for cells imaged within the 20- to 30-min time interval. ****, $p \leq 0.0001$.

MPs may function to supply a constant source of fluid to support the maintenance of a persistent RV. Consistent with this model, macropinocytosis is necessary for renitence.

Our work clarifies the kinetics of lysosomal damage and the sizes of molecules released from lysosomes following silica bead phagocytosis in macrophages. AW beads induced lysosomal damage as early as 15 min after incubation in both resting and LPS-treated BMM and permitted the release of small (3-kDa and, in some cases, 10-kDa) but not large (40- and 70-kDa) molecules. Our observations are consistent with those of other studies, in which incubation of macrophages with opsonized or unopsonized silica particles led to the release of 4-kDa fluorescent dextrans from endolysosomes for a limited period following phagocytosis (Joshi et al., 2015). The extent and timing of lysosomal damage we observed using AW beads also resembles that observed in macrophages infected with L.m., an intracellular bacterial pathogen that initiates its escape from phagolysosomes through the expression of a pore-forming toxin, listeriolysin O (LLO). Beginning ~15 min after L.m. infection, small perforations of the phagosomal membrane are formed that allow the release of molecular weight (522-Da) probes and expand over time to permit the release of larger (10-kDa) probes (Shaughnessy et al., 2006). Interestingly, membrane perforations induced by LLO resulted in the inhibition of fusion of L.m.-containing phagosomes with lysosomes (Shaughnessy et al., 2006). The block on maturation was thought to be timed to allow L.m. to prevent its delivery to the microbicidal environment of the lysosome before its escape into the cytosol. However, our observation of a block on fusion of RV-associated AW bead–containing phagosomes in the absence of infection suggests a similar strategy may be used by the host to prevent damage to lysosomes. Together, these observations suggest that AW beads induce physiologically relevant levels of phagolysosomal injury and that RVs form in response to small membrane perforations. Furthermore, renitence, which protects against the release of small but not large dyes, may have evolved as a mechanism of defense against small membrane perforations inflicted by pathogens.

Our assay for lysosomal damage allowed for sensitive detection of damage across a large sample of cells. Analyzing the distribution of damage measured within individual cells revealed that damage induced by AW beads in both resting and LPS-treated BMM was all-or-none. LPS activation conferred protection by limiting damage to the first 15 min of bead exposure and preventing the progression of damage in a protected subset of cells. Why certain subsets of LPS-treated BMM are susceptible to damage whereas others are resistant, however, is unknown. We considered whether the population of cells that resisted damage were more likely to contain RVs. However, based on preliminary analyses, no correlation exists between vacuole status after a 60-min incubation with AW beads and the propensity of cells for protection. While this result was surprising, it is possible that the vacuoles observed at 60 min are remnants of an earlier protective process and may not serve as a marker of protection for a given individual cell.

The striking morphological similarity of RVs to SPs, and their similar context for formation, suggests that the two structures are formed through related mechanisms. However, the two structures likely represent different topological compartments. That is, while SPs are phagosomes that have enlarged, likely due to macropinocytic influx into a bacteria-containing phagosome, RVs are formed adjacent to bead-containing phagosomes, and thus likely represent a distinct compartment. Whether RVs and adjoining bead-containing phagosomes are fused or exist as separate organelles is not known. The exact ultrastructural details of the spatial relationship of RVs and bead-containing phagosomes could theoretically be gained by electron microscopy, but the use of silica beads

(1) Macropinocytosis accompanies phagocytosis

Macropinosomes (MPs)

Tubular lysosomal network

(2) MPs associated with damaged phagosomes enlarge and persist ➔ RV formation

LAMP-1

Renitence vacuole (RV)

(3) Lysosomes interact with RVs, but not phagosomes, limiting damage to lysosomes

LAMP-1

LPS-activated macrophage

FIGURE 8: Model of cellular events involved in RV formation and protection against lysosomal injury. Sequence of events leading to RV formation and lysosomal damage protection in a representative LPS-activated macrophage. Lysosomes within LPS-activated macrophages assume a tubular lysosomal network (red). LPS-activated macrophages undergo macropinocytosis constitutively and upon particle phagocytosis. Upon internalization of a damaging particle, multiple MPs (green) accumulate around the incoming phagosome. In some cases, these MPs enlarge and persist. Persistent, periphagosomal MPs were identified as RVs. Whereas RVs fuse with lysosomes, as evidenced by their recruitment of LAMP-1 and acquisition of fluorescent probes preloaded into lysosomes, most phagosomes associated with RVs do not. Thus, RVs prevent the fusion of damaged phagosomes with intact lysosomes and thereby preserve lysosomal integrity.

as a damaging agent poses technical challenges for sample preparation. However, our light microscopic studies provide evidence that RVs and bead-containing phagosomes likely do not fuse. First, whereas RVs internalize fluid-phase dye by endocytosis and receive dye from prelabeled lysosomes, their neighboring bead-containing phagosomes do not. Second, the membranes of RVs are intact, as determined by their persistent acidity; adjacent phagosomes, because they contain a damaging particle, likely are damaged. If the two compartments were to fuse, damage likely would be transferred to RVs, which would no longer be able to maintain their low pH.

The relationship noted here between silica bead–containing phagosomes and their associated RVs resembles the relationship between *S. flexneri*–containing vacuoles and nearby MPs described in epithelial cells (Weiner *et al.*, 2016). *Shigella flexneri* induces its entry into nonphagocytic host cells by stimulating macropinocytosis. The process of invasion into host cells was long thought to involve macropinocytic uptake of the bacteria into a compartment called the bacteria-containing vacuole (BCV). While BCVs and MPs were thought to represent various stages of the same compartment, the work by Weiner *et al.* (2016) demonstrates that the two structures are distinct. Much as we saw during silica bead uptake in macrophages, *S. flexneri* infection of epithelial cells induced extensive membrane ruffling and MP formation near the BCV. As fluid-phase dye that labeled incoming MPs never labeled the BCV, the compartments were established as separate. Interestingly, in the setting of *S. flexneri* infection, macropinocytosis was found to be necessary for the destabilization of the BCV and *S. flexneri* escape, suggesting a role for macropinocytosis in facilitating membrane damage. Our work, in contrast, finds a membrane-protective role for macropinocytosis, as evidenced by its necessity for renitence. The two findings, however, are not necessarily conflicting. Instead, they support a larger model in which macropinocytosis represents a host protective response that 1) is induced by LPS activation or infection, 2) accompanies phagocytosis of particles or pathogens, 3) promotes membrane protection in the setting of injury, and 4) may be hijacked by some pathogens through the expression of virulence factors. As endocytic processes seem to limit the escape of some pathogens

(Schnettger *et al.*, 2017) but promote the pathogenesis of others (Alpuche-Aranda *et al.*, 1994; Watarai *et al.*, 2001; Weiner *et al.*, 2016), phagolysosomal integrity in the context of infection is likely determined by the outcome of the interactions between host and microbial factors.

This work examined responses of macrophages to phagocytosis-mediated membrane damage. Our model of silica bead–mediated lysosomal damage mimicked injury produced by pathogens and allowed for the direct interrogation of host responses to membrane damage. Using this reductionist approach, we discovered macropinocytosis and RV formation as activities accompanying particle phagocytosis in LPS-activated macrophages, activities whose significance during conventional phagocytosis is unclear, but that, in the setting of membrane injury, confer protection. As analogous processes occur in the context of infection, we believe that we have identified a general mechanism up-regulated by macrophage activation or infection that preserves endolysosomal integrity following phagocytic encounter with membrane-damaging threats.

MATERIALS AND METHODS
Materials
DMEM, RPMI 1640, fetal bovine serum (certified; FBS), GlutaMAX, penicillin–streptomycin, HBSS, Fdx (average molecular weight: 3, 10, 40, and 70 kDa), TRDx (70 kDa), nigericin, valinomycin, and 12-mm circular coverslips were purchased from ThermoFisher (Waltham, MA). Recombinant mouse M-CSF for macrophage differentiation was purchased from Peprotech (Rocky Hill, NJ), and that used for assays of macropinocytosis was purchased from R&D Systems (Minneapolis, MN). LPS from *S. Tm* (no. 225) was purchased from List Biological Laboratories (Campbell, CA). EIPA was purchased from Tocris (Minneapolis, MN). The 35-mm dishes with attached 14-mm coverglass were purchased from MatTek Corporation (Ashland, MA). BSA, 2-mercaptoethanol, and 0.01% poly-L-lysine (PLL) solution were purchased from Sigma.

Particle preparation
Three-micrometer silica dioxide microspheres were purchased from Microspheres-Nanospheres, a subsidiary of Corpuscular (Cold Spring, NY). Before use, the microspheres were acid-washed overnight in 1 N HCl and then rinsed several times with Milli-Q water. For generation of nondamaging beads, AW beads were first coated with 0.1 M PLL for 30 min, washed several times, then coated for 30 min with 5 mg/ml BSA.

Bone marrow macrophage isolation and culture
C57BL6/J mice were purchased from the Jackson Laboratory (Bar Harbor, ME). BMM were obtained as previously described (Davis *et al.*, 2012), with slight modification. Briefly, marrow cells extruded from mouse femurs were differentiated into macrophages through culture for 6–8 d in DMEM supplemented with 20% FBS, 50 ng/ml recombinant M-CSF, 1% GlutaMAX, 37 µM 2-mercatpoethanol, and 10 U/ml penicillin–streptomycin. All animal-related procedures were approved by the University of Michigan Committee on Use and Care of Animals.

Cell culture and stimulation

BMM were plated onto glass-bottom microwell dishes (MatTek) in RPMI 1640 containing 10% FBS, 1% GlutaMAX supplement, and 10 U/ml penicillin–streptomycin. For labeling of lysosomes, BMM were incubated overnight with 150 μg/ml Fdx of various molecular weights (3, 10, 40, or 70 kDa), and the next day were rinsed in Ringer's buffer and returned to unlabeled media for at least 3 h before the start of imaging. LPS (100 ng/ml) was added to cells during both the overnight pulse and chase periods. Lysosomal damage was induced by feeding BMM 3-μm AW beads in RPMI lacking serum for 60 min. AW beads were added at a concentration empirically determined to result in uptake of three to four beads per cell on average by both resting and LPS-activated BMM. All analyses of damage were performed on cells that had internalized three to seven beads per cell.

In studies assessing the effect of macropinocytosis on renitence, macropinocytosis was stimulated and inhibited with the following treatments. To stimulate macropinocytosis, M-CSF (200 ng/ml) was included in the media during the time of AW-bead incubation. To inhibit macropinocytosis, BMM were pretreated with EIPA (25 μM) for 30 min before the start of bead incubation and then fed beads in RPMI containing 25 μM EIPA.

Measurement of lysosomal damage by ratiometric imaging

Damage to lysosomes was measured as previously described, using an assay for ratiometric measurement of pH (Davis and Swanson, 2010; Davis et al., 2012). BMM containing Fdx-labeled lysosomes were imaged by fluorescence microscopy after a 60-min incubation in the presence or absence of AW or BSA-coated beads. Images were acquired on a Nikon TE300 inverted microscope equipped with a mercury arc lamp, Plan-Apochromat 60×, 1.4 NA objective, cooled digital CCD camera (Quantix Photometrics, Tucson, AZ), temperature-controlled stage, and a fluorescein isothiocyanate (FITC) ratiometric dichroic mirror (Chroma Technology, Bellows Falls, VT). For each field of cells imaged, three images were acquired: one phase-contrast image, which allowed enumeration of bead number per cell; and two fluorescence images, from which pH information was obtained. Fluorescence images of Fdx were captured using a single emission filter centered at 535 nm and two different excitation filters, centered at 440 or 490 nm. Image acquisition and analysis were performed using MetaMorph software (Molecular Devices, Sunnyvale, CA).

The fluorescent signal emitted by Fdx is dependent on pH following excitation at 490 nm, but relatively insensitive to pH when excited at 440 nm. Taking the ratio of fluorescence intensities captured in the 490 and 440 channels respectively (i.e., Fdx ex. 490 nm/Fdx ex. 440 nm) yields volume-corrected pH information for each pixel in the image. To convert 490/440 nm ratios into pH values, we generated a calibration curve by measuring 490/440 nm ratio values in BMM containing Fdx-labeled lysosomes clamped to a fixed pH (from 3.0 to 9.0) in clamping buffers (130 mM KCl, 1 mM MgCl$_2$, 15 mM HEPES, 15 mM MES) containing nigericin (10 μM) and valinomycin (10 μM). Average 490/440 nm ratio values were determined for each pH, and these data were fitted to a four-variable sigmoidal standard curve using GraphPad PRISM software (GraphPad Software, La Jolla, CA).

Cellular pH maps were generated by using a color look-up table to assign to each pixel in the image a color corresponding to its pH value, with warm colors assigned to acidic regions and cool colors assigned to pH-neutral regions.

Release of Fdx from lysosomes was indicated by the presence of dye in cellular regions whose pH was greater than 5.5. Masks representing pixels whose pH was greater than 5.5 in 490/440 nm ratiometric images were created and transferred to 440-nm excitation images. Owing to the insensitivity of Fdx excitation to pH at this wavelength, fluorescence intensity values in these images are considered to be proportional to the amount of Fdx in each pixel. For determination of the fraction of Fdx released from lysosomes within individual cells, the 440-nm fluorescence intensities of pixels whose pH was greater than 5.5 were summed, and this value was divided by the total 440-nm fluorescence intensity for a given cell.

Analysis of vacuole frequency

RV frequency was determined in acquired images of resting or LPS-treated BMM from which measurements of lysosomal damage were made. Images from experiments in which BMM were fed AW or BSA-coated beads for 60 min were scored for the presence or absence of RVs. Vacuolar structures observed within cells were scored as RVs by the following criteria: 1) appearance on the phase-contrast image as a circumscribed phase-dense region adjacent to an internalized bead, and 2) presence of Fdx within the structure. RV frequency was quantified as the percent of cells containing one or more vacuoles within a given condition. All cells containing at least one bead were included in the analysis.

MP counting assay

For measurement of macropinocytosis, resting or LPS-treated BMM plated on 12-mm circular coverslips were pulsed for 10 min with 70-kDa Fdx (0.5 mg/ml). In control conditions, macropinocytosis was stimulated by inclusion of M-CSF (200 ng/ml) during the time of the Fdx pulse or inhibited by 30 min pretreatment with EIPA (25 μM) before the start of the pulse. Cells were gently washed with HBSS to remove uningested probe, fixed for 30 min at 37°C with fixation buffer (75 mM lysine-HCl, 37.5 mM Na$_2$HPO$_4$, 4.5% sucrose, 2% paraformaldehyde, 10 mM sodium periodate), and imaged by fluorescence microscopy. MetaMorph software was used to merge phase-contrast and background-subtracted Fdx images. The number of MPs per cell was determined by scoring the number of Fdx-positive, phase-bright vesicles in the merged images. At least 25 cells were scored for each experiment.

Time-lapse video microscopy

BMM plated onto glass-bottom microwell dishes were incubated overnight with either LY (1 mg/ml) or 70-kDa TRDx (25 or 50 μg/ml) in media containing 100 ng/ml LPS and then chased in unlabeled media for at least 3 h the next day. Cells containing LY-labeled lysosomes were fed AW beads and immediately mounted for imaging. Cells containing TRDx-labeled lysosomes were fed AW beads and 0.5 mg/ml 70-kDa Fdx for 5 min, washed, and mounted for imaging. Excitation and emission wavelengths used were as follows: LY (ex. 430 nm–em. 535 nm), TRDx (ex. 572 nm–em. 632 nm), and Fdx (ex. 490 nm–em. 535 nm). Images were collected on a Nikon TE inverted microscope equipped with ECFP-EYFP-mCherry and DAPI-FITC-Texas Red dichroic mirrors (Chroma Technology). LY fluorescence images were collected using the former, and Fdx and TRDx were collected using the latter. Images for each condition analyzed were collected in at least three independent experiments.

Quantitative analysis of the frequency of phagosome-lysosome fusion

BMM plated on glass-bottom microwell dishes were incubated overnight with 25 μg/ml TRDx (70 kDa) and 100 ng/ml LPS and then chased in unlabeled media for at least 3 h the next day. Cells were fed AW beads for 60 min, washed to remove noninternalized particles, and then mounted for imaging. Over a 10-min

imaging interval, several still frames of phase-contrast and TRDx (ex. 572 nm–em. 632 nm) images were collected. AW bead–containing phagosomes observed on phase-contrast images were determined to be RV-associated or not, and then scored for their fusion with lysosomes, with fusion judged as localization of TRDx fluorescence around beads. At least 200 phagosomes were analyzed per experiment in three independent experiments.

Plasmids and transfection

YFP-Rab5a and CFP-LAMP-1 plasmids were described previously (Henry *et al.*, 2006). The plasmid pmCherry-C1 (Takara Bio USA, Mountain View, CA) was used for expression of free mCherry. All plasmids were purified using an EndoFree Plasmid Purification Kit (Qiagen, Venlo, Netherlands). BMM were transfected with all three plasmids using a Nucleofector kit for Mouse Macrophages (Lonza, Basel, Switzerland) according to the manufacturer's protocol. Following transfection, macrophages were seeded onto glass-bottom microwell dishes in RPMI 1640 containing 10% FCS, 1% glutamax, and 20 U/ml penicillin–streptomycin. Cells were incubated overnight in media containing 100 ng/ml LPS.

YFP-Rab5a and CFP-LAMP-1 imaging

Transfected LPS-treated BMM were incubated with AW beads for either 5 min or 20 min in RPMI 1640 media lacking phenol red. Cells were then washed to remove noninternalized beads and mounted for imaging. Still frames of phase-contrast, mCherry, YFP, and CFP images were collected over a 5-min interval in coverslips incubated with AW beads for 5 min, and over a 10-min interval in coverslips incubated with AW beads for 20 min. Imaging was performed on a Nikon TE300 inverted microscope using an ECFP-EYFP-mCherry dichroic mirror and the following excitation and emission filter sets: mCherry (ex. 572 nm–em. 632 nm), YFP (ex. 500 nm–em. 535 nm), and CFP (ex. 440 nm–em. 470 nm). Cells were selected for imaging only if they expressed all three probes and harbored characteristic vacuoles as defined in Figure 3.

Ratiometric imaging analysis

All fluorescence images used for ratiometric analysis (i.e., YFP-Rab5a, CFP-LAMP-1, and mCherry) were first corrected for camera bias and uneven illumination as previously described (Davis and Swanson, 2010). To discard signal from regions outside of fluorescent cell areas, a binary threshold was applied over the cell using the mCherry component image.

The recruitment of YFP-Rab5a or CFP-LAMP-1 to RVs was assessed in ratiometric images generated by dividing the fluorescent signal in images of either fluorescent chimera by the fluorescent signal for mCherry (i.e., YFP-Rab5a/mCherry or CFP-LAMP-1/mCherry). This approach corrects for variations in optical path length owing to differences in cell thickness. The ratio images generated thus report the relative concentration of a specific fluorescent chimera in any given region of the cell normalized for cell thickness. Phase-contrast images were used to identify the position of RVs. High-intensity signal on the ratio image in regions corresponding to an RV was judged as positive recruitment of a given probe to the RV.

Statistical methods

Statistical analysis for all experiments was performed using Graph-Pad Prism software (GraphPad Software). Lysosomal damage levels between groups were compared using two-way analysis of variance (ANOVA) with multiple comparisons (Tukey's test; Figures 1, 2, 3, and 5). Comparison of vacuole frequency between groups was performed using a two-tailed, unpaired *t* test (Figure 3B) or two-way

ANOVA with multiple comparisons (Tukey's test; Figure 3D). A two-tailed, unpaired *t* test with Welch's correction was applied to compare the extent of MP formation between groups (Figure 5A) and the proportion of RV versus non–RV associated phagosomes undergoing fusion with TRDx-positive lysosomes (Figure 6C). Comparison of the proportion of vacuoles labeled with Rab5 and/or LAMP-1 after various time points of bead incubation was performed using two-way ANOVA with multiple comparisons (Tukey's test; Figure 7C).

REFERENCES

Alpuche-Aranda CM, Racoosin EL, Swanson JA, Miller SI (1994). *Salmonella* stimulate macrophage macropinocytosis and persist within spacious phagosomes. J Exp Med 179, 601–608.

Boya P, Kroemer G (2008). Lysosomal membrane permeabilization in cell death. Oncogene 27, 6434–6451.

Case ED, Smith JA, Ficht TA, Samuel JE, de Figueiredo P (2016). Space: a final frontier for vacuolar pathogens. Traffic 17, 461–474.

Davis MJ, Gregorka B, Gestwicki JE, Swanson JA (2012). Inducible renitence limits *Listeria monocytogenes* escape from vacuoles in macrophages. J Immunol 189, 4488–4495.

Davis MJ, Swanson JA (2010). Technical advance: Caspase-1 activation and IL-1β release correlate with the degree of lysosome damage, as illustrated by a novel imaging method to quantify phagolysosome damage. J Leukoc Biol 88, 813–822.

Henry R, Shaughnessy L, Loessner MJ, Alberti-Segui C, Higgins DE, Swanson JA (2006). Cytolysin-dependent delay of vacuole maturation in macrophages infected with *Listeria monocytogenes*. Cell Microbiol 8, 107–119.

Hornung V, Bauernfeind F, Halle A, Samstad EO, Kono H, Rock KL, Fitzgerald KA, Latz E (2008). Silica crystals and aluminum salts activate the nalp3 inflammasome through phagosomal destabilization. Nat Immunol 9, 847–856.

Joshi GN, Goetjen AM, Knecht DA (2015). Silica particles cause NADPH oxidase-independent ros generation and transient phagolysosomal leakage. Mol Biol Cell 26, 3150–3164.

Levine B, Mizushima N, Virgin HW (2011). Autophagy in immunity and inflammation. Nature 469, 323–335.

Racoosin EL, Swanson JA (1989). Macrophage colony-stimulating factor (rM-CSF) stimulates pinocytosis in bone marrow-derived macrophages. J Exp Med 170, 1635–1648.

Racoosin EL, Swanson JA (1993). Macropinosome maturation and fusion with tubular lysosomes in macrophages. J Cell Biol 121, 1011–1020.

Schnettger L, Rodgers A, Repnik U, Lai RP, Pei G, Verdoes M, Wilkinson RJ, Young DB, Gutierrez MG (2017). A Rab20-dependent membrane trafficking pathway controls *M. tuberculosis* replication by regulating phagosome spaciousness and integrity. Cell Host Microbe 21, 619–628.e615.

Schroder K, Tschopp J (2010). The inflammasomes. Cell 140, 821–832.

Shaughnessy LM, Hoppe AD, Christensen KA, Swanson JA (2006). Membrane perforations inhibit lysosome fusion by altering pH and calcium in *Listeria monocytogenes* vacuoles. Cell Microbiol 8, 781–792.

Swanson JA, Watts C (1995). Macropinocytosis. Trends Cell Biol 5, 424–428.

Watarai M, Derre I, Kirby J, Growney JD, Dietrich WF, Isberg RR (2001). *Legionella pneumophila* is internalized by a macropinocytotic uptake pathway controlled by the Dot/Icm system and the mouse Lgn1 locus. J Exp Med 194, 1081–1096.

Weiner A, Mellouk N, Lopez-Montero N, Chang YY, Souque C, Schmitt C, Enninga J (2016). Macropinosomes are key players in early *Shigella* invasion and vacuolar escape in epithelial cells. PLoS Pathog 12, e1005602.